IN-PLANE ELASTIC PROPERTY CHARACTERIZATION IN COMPOSITE PLATES

O. I. Lobkis, D. E. Chimenti, Han Zhang, and M. Rudolph

Center for Nondestructive Evaluation and
Aerospace Engineering & Engineering Mechanics Dept
Iowa State University
Ames IA 50011

INTRODUCTION

In the elastic property characterization of composite laminates with liquid-coupled ultrasound, the stiffnesses that are most easily and accurately measured in conventional single-sided reflection geometries are those of least interest to structural design engineers. Typical elastic wave measurements produce detailed maps of out-of-plane longitudinal stiffnesses, average laminate shear constants, and even mixed stiffnesses, such as C_{13}, C_{23}, etc, although these latter can be difficult to infer accurately [1]–[6]. (Further background on this topic can be found in recent reviews [7], [8].) This portion of the stiffness matrix is, however, of relatively little interest to most designers of composite structure. Of far greater interest is the longitudinal in-plane stiffness, since this property controls the effect of tensile and compressive forces on the laminate structure. Additionally, the laminate bending stiffness is another useful material property, but in this paper we concentrate on measuring the in-plane longitudinal stiffness C_{11}.

The difficulty in assessing the in-plane properties arises for two reasons. The in-plane stiffness C_{11} influences a relatively small portion of the reflection spectrum in a way that it can be unequivocally inferred from measurements. Moreover, this portion of the reflection spectrum cannot be easily accessed in conventional time/frequency studies. It is, in particular, the low-frequency behavior of the lowest order symmetric Lamb mode S_0 that depends on C_{11}. Moreover, for the special case of highly anisotropic media such as composite laminates the S_0 phase velocity in this regime depends almost exclusively on C_{11}. The case is illustrated in Fig. 1 [9]. Below $fd \approx 0.5$ mm.MHz the S_0 wavespeed is nearly constant and strongly dependent only on C_{11}. This fortunate circumstance can be exploited to infer C_{11} from a simple liquid-coupled reflection measurement.

Review of Progress in Quantitative Nondestructive Evaluation, Vol. 17
Edited by D.O. Thompson and D.E. Chimenti,, Plenum Press, New York, 1998

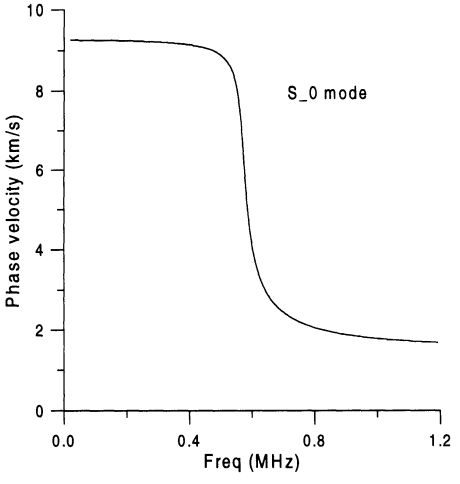

Figure 1. Dispersion curve for the S_0 Lamb mode of a uniaxial composite laminate showing the nearly dispersionless behavior below $fd \approx 0.5$ mm.MHz. In a composite this plateau depends almost exclusively on C_{11}.

THEORETICAL SUMMARY

We assume the laminate lies in the x_1x_2 plane with the origin of coordinates at the center of the plate. The x_3 direction then is normal to the plane of the laminate. In the standard Lamb wave problem all tractions are taken to vanish at the two free laminate surfaces $x_3 = \pm h$, where h is the laminate half-thickness. In the low frequency limit, however, the x_3 tractions will vanish throughout the laminate, and the particle motion will be dominated by in-plane displacements. Using the constitutive equations for an orthotropic laminate with particle motion in the x_1x_3 plane only, we have for the stresses,

$$\begin{aligned} \sigma_{13} &= C_{55}\left(\frac{\partial u_1}{\partial x_3} + \frac{\partial u_3}{\partial x_1}\right) \to 0 \\ \sigma_{33} &= C_{13}\frac{\partial u_1}{\partial x_1} + C_{33}\frac{\partial u_3}{\partial x_3} \to 0 \qquad x_3 \in [-h, +h]\,. \end{aligned} \tag{1}$$

Together, these equations imply that relations exist between the x_1 and x_3 displacement gradients,

$$\begin{aligned} \frac{\partial u_3}{\partial x_1} &= -\frac{\partial u_1}{\partial x_3} \\ \frac{\partial u_3}{\partial x_3} &= -\left(\frac{C_{13}}{C_{33}}\right)\frac{\partial u_1}{\partial x_1}\,, \end{aligned} \tag{2}$$

where again, these relations apply throughout laminate thickness. The linear elastic wave equation for u_1, with wave motion confined to the x_1x_3 plane, is

$$\rho\frac{\partial^2 u_1}{\partial t^2} = C_{11}\frac{\partial^2 u_1}{\partial {x_1}^2} + C_{55}\frac{\partial^2 u_1}{\partial {x_3}^2} + C_{55}\frac{\partial^2 u_3}{\partial x_1 \partial x_3} + C_{13}\frac{\partial^2 u_3}{\partial x_3 \partial x_1}\,. \tag{3}$$

The results of Eqs. (2) can be inserted into Eq. (3), eliminating all but dependence on u_1 and its x_1 gradient. Assuming a time dependence of $\exp(-i\omega t)$ (ω is the angular frequency), the result is a simple differential equation for u_1

$$-\rho\omega^2 u_1 = C_{11}\frac{\partial^2 u_1}{\partial {x_1}^2} - \frac{C_{13}^2}{C_{33}}\frac{\partial^2 u_1}{\partial {x_1}^2}, \tag{4}$$

that can be solved by substituting the formal solution $u_1 = U_1 \exp(i\xi x_1)$. This substitution leads to a condition on the plate wavespeed $V_{\rm pl}\,(= \omega/\xi)$,

$$\rho V_{\rm pl}^2 = C_{11} - \frac{C_{13}^2}{C_{33}}. \tag{5}$$

This relation is particularly fortuitous for composite laminates, where the elastic anisotropy can lead to ratios of 8 or 10 between C_{11} and C_{33}, accompanied by an even smaller value of C_{13}. For the case of a uniaxial laminate (x_1 is the fiber direction) of 65% AS/4 fibers in 3501 epoxy, $C_{11} \approx 140$ GPa, $C_{13} \approx 2.7$ GPa, and $C_{33} \approx 10$ GPa, the error in ignoring the second term in Eq. (5) compared to the first is less than 1%. Because of this circumstance we may take $V_{\rm pl}$ to be wholly dependent on C_{11} with negligble loss of accuracy. In other laminate configurations, as we shall see below, the error incurred by neglecting this term can be larger, but essentially never exceeding 10%.

MEASUREMENT METHOD

The handy result in Eq. (5) above can be exploited only if we can find a way to make an accurate local measurement of the low-frequency S_0 plate wavespeed. As we have seen above, time/frequency domain methods do not yield a sensitive measurement since the mode is nearly dispersionless (constant velocity with frequency) in the regime of interest. Instead, we take advantage of the spatial spectrum of the finite-beam transducer over a limited, but information-rich, zone of the dispersion curve. We perform a spatial scan of the receiver with respect to the transmitter, as illustrated in Fig. 2, where the voltage is measured at each of 60 or 80 discrete positions. The only important criterion is that the step size should be much less than the guided mode wavelength in the plate ($\lambda_{\rm pl} = 2\pi V_{\rm pl}/\omega$). At the low frequencies we use in this work, this length works out to about 1 mm. It is important, however, that all geometric parameters, other than the transducer separation parameter x (shown in Fig. 2) be held constant during the scan. An example of a scan showing the real and imaginary parts of the transducer voltage for a uniaxial composite laminate with an incident angle of 10° is shown in Fig. 3.

Once the data are acquired, a spatial frequency spectrum can be constructed from the scanned voltage values according to

$$S(\theta;\alpha) = \int_{-\infty}^{\infty} V(x;\alpha)\exp[-i\,(\kappa_f \sin\theta)x]\,dx\,. \tag{6}$$

Here, θ is the phase-match angle (explained below), α is the beam incident angle, x is the transducer separation parameter (shown in Fig. 3), and κ_f is the wavenumber in the fluid. In acquiring the voltage data it is critical to preserve the phase information; this task is accomplished by collecting the entire 50-μ sec monochromatic toneburst and performing a time/frequency Fourier transform on it, extracting only that

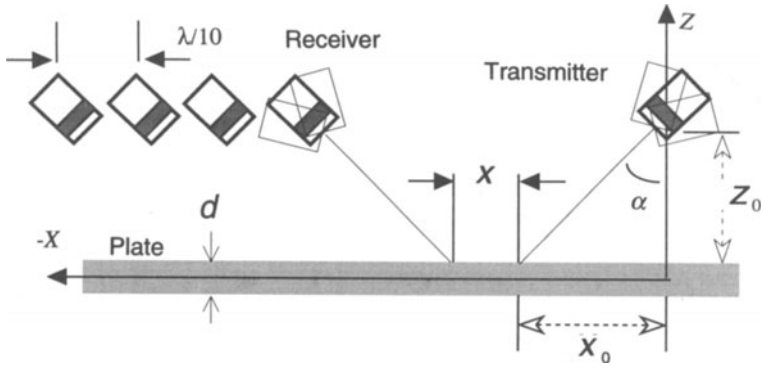

Figure 2. Schematic diagram showing the inplane property measurement procedure. The transducer separation parameter is x.

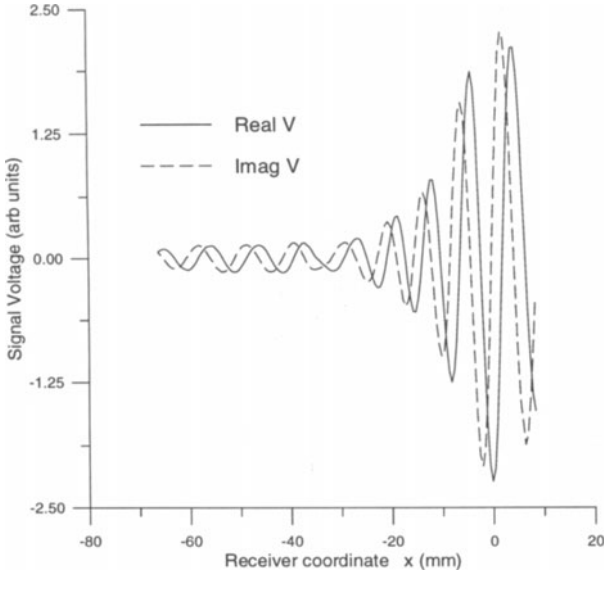

Figure 3. Receiver position scan performed according to Fig. 2 showing real and imaginary parts of voltage for a uniaxial composite laminate with an incident angle of 10°.

frequency component corresponding to the toneburst center frequency. The result at every x receiver position is the term $V(x;\alpha)$ in the equation above. The real part of this voltage is illustrated in Fig. 3. The complex voltages for all the positions in the scan are then subjected to a spatial Fourier transform, as indicated in Eq. (6).

The result of this operation is dependent on the transducer beam spread. Were the plate to be perfectly rigid (unity reflection coefficient), then the result would be only the incident spatial beam spectrum, or a function equal to the combined directivity functions of the transmitter and receiver. With an *elastic* plate the plate reflection properties will be superimposed on the beam function. In this case the S_0 guided wave reflection zero gives rise to a sharp decrease in the function $S(\theta;\alpha)$ at the phase-match angle corresponding to the mode phase velocity through Snell's law, $\kappa_f \sin\theta = \omega/V_{\rm pl}$. It is from this relationship and Eq. (5) that we extract our in-plane C_{11} property information. Depending on the transducer geometry, the frequency, and the initial estimate of C_{11}, however, more than one scan at different incident angles α may be needed to cover the angular range of interest. In that case, the data for each angle can simply be summed incoherently,

$$S(\theta) = \sum_{\alpha_n} S(\theta, \alpha_n)\,, \tag{7}$$

obtaining only in the magnitude of the $S(\theta)$ function.

RESULTS AND DISCUSSION

Spatial Fourier transforms according to Eq. (6) of data taken at a single incident angle $\alpha = 10°$ for a uniaxial T300/CG-914 $[0]_8$ graphite-epoxy laminate are shown in Fig. 4. The ultrasonic frequency is 1.0 MHz. The overall behavior in this curve is determined by the transducer geometry and frequency. The dip near a phase-match angle of 9° is caused by the presence of the S_0 guided wave mode, whose reflection zero causes the signal decrease. The estimate of C_{11} (along the fiber direction) from these data is 142 GPa. The value inferred for this laminate from related, but rather different experiments, is 145 Gpa, which compares favorably with our current measurement, although both these values are low when compared to generic tabular data for a similar material system, T300/5208 [12].

The formalism developed above generally applicable beyond uniaxial laminates. A goal of this work is to demonstrate that the more complicated, industrially relevant, layups can also be accurately measured using this method. Therefore, we have examined a biaxial graphite-epoxy laminate $[0,90]_{3S}$ of AS/4-3501, which has been independently characterized by acid digestion. The results are shown for 0.5 MHz in Fig. 5, and the clear indication of the S_0 mode is a minimum near 13°. From lamination theory [12] the in-plane longitudinal stiffness of a biaxial laminate is given by

$$A_{11} = U_1 + (v_0 - v_{90})U_2 + U_3\,, \tag{8}$$

where the U_i are tabulated linear combinations of single-ply stiffness matrix elements, v_ϕ is the volume fraction of fibers in the ϕ direction, and A_{IJ} is the inplane property matrix. For balanced laminates, such as we study here, $(v_0 - v_{90})$ vanishes. Using the tabular data (our actual fiber volume fraction is close to that assumed in the table), we obtain an estimate of 73.9 GPa. This result is quite close to our measured value of

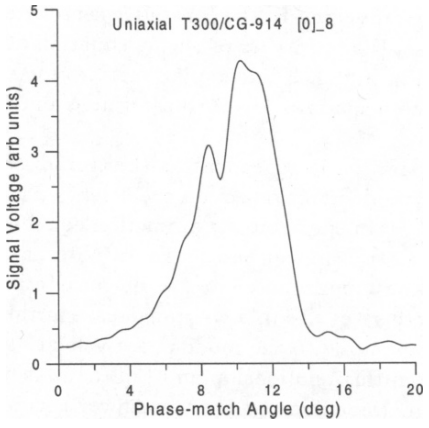

Figure 4. Reflection function $S(\theta)$ versus phase-match angle for a uniaxial $[0]_8$ graphite-epoxy laminate of T300/CG-914. The minimum in the curve near 9° result from phase matching incident wave to S_0 guided wave mode. Data are shown for $\alpha = 10°$; the rf frequency is 1.0 MHz.

71.3 GPa, although in this case the ratio of C_{13}^2/C_{33} is a larger fraction of C_{11} than for the uniaxial laminate. The absolute size of the out-of-plane normal stiffness C_{33} for a given material system does not, of course, change with layup sequence.

The last example is perhaps the most ubiquitous layup sequence, since it approximates the familiar properties of monolithic structural materials. The stacking sequence of $[0,+45,-45,90]_{2S}$ leads to inplane properties that are approximately isotropic, and this sequence is called quasi-isotropic. In this case the value of C_{13} may be slightly larger and C_{13}^2/C_{33} will be proportionately larger than C_{11}, which is decreasing as the fibers are distributed in several directions. Nonetheless, the intrinsic stiffness ratios are large enough that the error in ignoring the C_{13} contribution will still generally be acceptable.

Figure 6 shows the summed results at 0.5 MHz for three measurements at incident angles of $\alpha = 14°$, 15°, and 16°. The material system is again AS/4-3501. Here, the sharp minimum is near a phase-match angle of 14.8°, leading to an experimental determination of C_{11} of 54.9 GPa. This value is, in fact, about 10% different from the estimate of lamination theory, $A_{11} = 59.7$ GPa. But, such an outcome might be expected, since we consciously ignore the contribution to C_{11} of C_{13}^2/C_{33}, alhtough this term should still be small. Another possibility is that the layup sequence is not precise, leading to uncertainties in the inplane stiffness. It would be possible, in principle, to improve the inplane stiffness estimate; it would be necessary, however, to know in advance the laminate stacking sequence.

Finally, let us consider the robustness of the procedure. To show that neither the precise choice of angle, nor the exact equality between transmitter angle and receiver angle are critical to reproducible results, we present in Fig. 7 the results of several scans performed on the uniaxial specimen. The different curves of $S(\theta)$ are shown individually and not summed for transmission and reception at 8°, 9°, and 10°, as

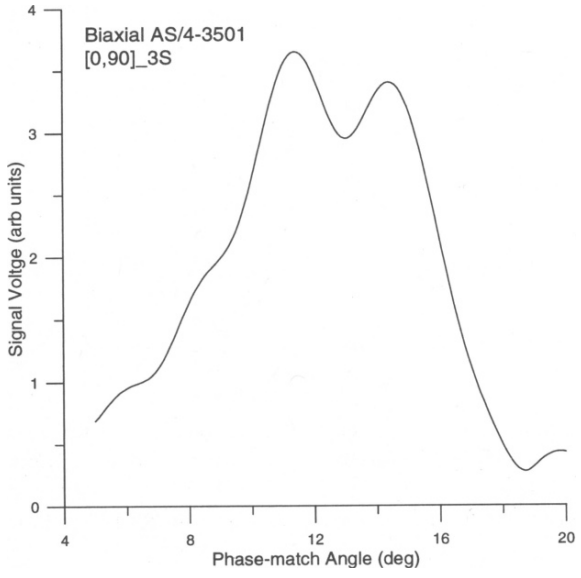

Figure 5. Reflection function $S(\theta)$ versus phase-match angle for a biaxial $[0,90]_{3S}$ graphite-epoxy laminate of AS/4-3501. The minimum in the curve near 13° is the result of phase matching of the incident wave to the S_0 guided wave mode. Data are shown summed for $\alpha = 11°$, 12°, and 13°. The frequency is 0.5 MHz.

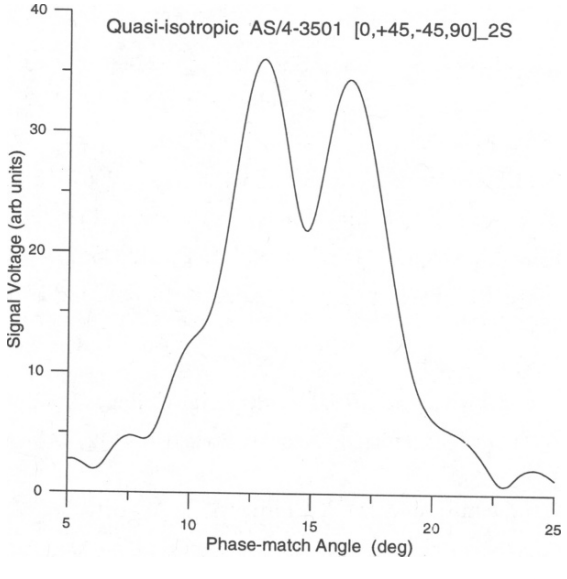

Figure 6. Reflection function $S(\theta)$ versus phase-match angle for a quasi-isotropic $[0,+45,-45,90]_{2S}$ graphite-epoxy laminate of AS/4-3501. The minimum in the curve near 14.8° is the result of phase matching of the incident wave to the S_0 guided wave mode. Data are shown summed for $\alpha = 14°$, 15°, and 16°. The frequency is 0,5 MHz.

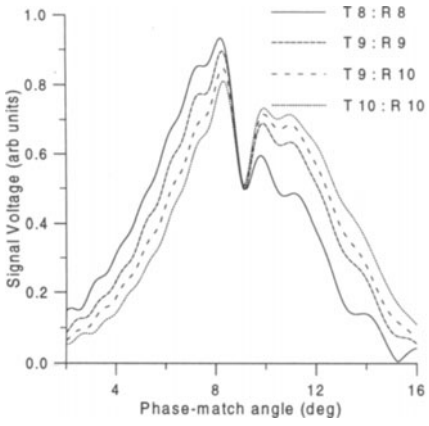

Figure 7. Reflection functions $S(\theta;\alpha)$ versus phase-match angle for uniaxial $[0]_8$ AS/4-3501 laminate at $f = 0.5$ MHz. Curves correspond to different transmitter-receiver setup, indicated in legend. Minima in curves near 9° show phase matching to S_0 guided wave. Same minima for all curves indicates method's robustness.

indicated in the figure legend. The data recorded as the wide-dash curve, however, have been acquired with the transmitter at 9° and the receiver at 10°. In all cases the minimum is reproducibly located at the angle used to derive the estimate of 142 GPa from Fig. 4 above. This important result implies that our method has significant application potential in the industrial environment, where precise transducer alignments are not always feasible.

REFERENCES

1. V. Dayal and V. K. Kinra, J. Acoust. Soc. Am. 85, 2268–76, (1989).
2. D. E. Chimenti and A. H. Nayfeh, J. Nondestruct. Eval. 9, 51–69 (1990).
3. R. A. Kline, J. Eng. Mat. Tech. 112, 218–22, (1990).
4. M. Deschamps and B. Hosten, J. Acoust. Soc. Am. 91, 2007–15, (1992).
5. Y. Bar-Cohen, AK Mal, and SS Lih, Mater. Eval. vol51, 1285–96 (1993).
6. J. L. Rose, A. Pilarski, and J. J. Ditri, J. Reinf. Plast. Comp. 12, 536–44 (1993).
7. A. H. Nayfeh, *Wave Propagation in Layered Anisotropic Media*, (North-Holland, Amsterdam, 1995).
8. D. E. Chimenti, Appl. Mech. Rev. 50, 247–84 (1997).
9. Curve was produced with *DISPERSE*©, Imperial College, London, England.
10. O. I. Lobkis and D. E. Chimenti, J. Acoust. Soc. Am. 102, 143–49 (1997); *ibid.* 102, 150–59 (1997).
11. O. I. Lobkis, A. Safaeinili, and D. E. Chimenti, J. Acoust. Soc. Am. 99, 2727–36 (1996).
12. S. W. Tsai and H. T. Han, *Introduction to Composite Materials*, (Technomic, Lancaster, PA, 1980).